Journal of Sensor Science and Technology
Vol. 30, No. 4 (2021) pp. 191-195
http://dx.doi.org/10.46670/JSST.2021.30.4.191
pISSN 1225-5475/eISSN 2093-7563

Highly sensitive xylene sensors using Fe_2O_3-$ZnFe_2O_4$ composite spheres

Jin Fang Chan[1,*], Jae Kyoung Jeon[1,*], Young Kook Moon[1,*], and Jong-Heun Lee[1,+]

Abstract

Pure $ZnFe_2O_4$ and Fe_2O_3-$ZnFe_2O_4$ hetero-composite spheres were prepared by ultrasonic spray pyrolysis of a solution containing Zn- and Fe-nitrates. Additionally, the sensing characteristics of these spheres in the presence of 5 ppm ethanol, benzene, *p*-xylene, toluene, and CO (within the temperature range of 275-350 °C) were investigated. The Fe_2O_3-$ZnFe_2O_4$ hetero-composite sensor with a cation ratio of [Zn]:[Fe]=1:3 exhibited a high response (resistance ratio = 140.2) and selectivity (response to *p*-xylene/response to ethanol = 3.4) to 5 ppm *p*-xylene at 300 °C, whereas the pure $ZnFe_2O_4$ sensor showed a comparatively lower gas response and selectivity. The reasons for the superior response and selectivity to *p*-xylene in Fe_2O_3-$ZnFe_2O_4$ hetero-composite sensor were discussed in relation to the electronic sensitization due to charge transfer at Fe_2O_3-$ZnFe_2O_4$ interface and Fe_2O_3-induced catalytic promotion of gas sensing reaction. The sensor can be used to monitor harmful volatile organic compounds and indoor air pollutants.

Keywords : Gas sensors, Oxide semiconductors, Fe_2O_3-$ZnFe_2O_4$, Xylene, Ultrasonic spray pyrolysis.

1. INTRODUCTION

Metal oxide semiconductors with distinctive advantages such as high response, simple structure, and rapid response speed have been widely used to detect toxic, explosive, and harmful gases [1,2]. The gas sensing characteristics can be controlled by loading noble metal or oxide catalysts [3-5], designing nanostructures [6,7], controlling the composition of sensing materials [8], and establishing hetero-composites [9]. From the viewpoint of compositional control, multinary oxides such as spinels and perovskites are promising gas sensing materials [10] since various combinations between two cations with different catalytic activity and acid-base properties can be used to achieve new functionality of gas sensors [9]. In addition, the formation of hetero-composites between multinary oxide and other oxide provides further control of gas sensing characteristics [11].

Ultrasonic spray pyrolysis is a process to convert the droplets of a precursor solution to oxides, which enables the facile preparation of oxide spheres with complex composition [12]. In the present contribution, pure and Fe_2O_3-loaded $ZnFe_2O_4$ spheres were prepared by ultrasonic spray pyrolysis of a solution containing Zn-nitrate and Fe-nitrate, and their gas sensing characteristics were investigated. The Fe_2O_3-loaded $ZnFe_2O_4$ spheres prepared from the precursor solutions with a cation ratio of [Zn]:[Fe]=1:3 exhibited a superior gas response and selectivity to *p*-xylene. The main focus of this study was understanding the key parameters to determine gas sensing characteristics and gas sensing mechanism.

2. EXPERIMENTAL

2.1 Synthesis of sensing materials

$ZnFe_2O_4$ spheres were prepared by one-pot ultrasonic spray pyrolysis of an aqueous solution (200 mL) containing zinc nitrate hexahydrate (1.98 g, $Zn(NO_3)_2 6{\cdot}H_2O$, 99%, Sigma-Aldrich, USA), iron(III) nitrate nonahydrate (5.38 g, $Fe(NO_3)_3{\cdot}9H_2O$, 98%, Sigma-Aldrich, USA), and citric acid monohydrate (3.84 g, $C_6H_8O_7{\cdot}H_2O$, 99.5%, Sigma-Aldrich, USA) (Fig. 1(a)). The molar ratio between Zn and Fe ([Zn]:[Fe]) was fixed to 1:2. The droplets generated by five ultrasonic transducers were transferred into a high-temperature (700 °C) tubular reactor (length: 1200 mm, inner diameter: 50 mm) by air at a flow rate of 10 L/min. The droplets were converted into precursor powders during spray pyrolysis and collected in a Teflon bag filter. The $ZnFe_2O_4$ spheres were prepared by annealing the precursor powders at 600 °C for 2 h in air. $ZnFe_2O_4$-Fe_2O_3 nanocomposite spheres with composition of

[1] Department of Materials Science and Engineering, Korea Unversity, Anam Dong, Seongbuk Gu, Seoul 02841, Korea
*These authors are contrubuted equally to this work
+Corresponding author: jongheun@korea.ac.kr
(Received: Jun. 28, 2021, Revised: Jul. 21, 2021, Accepted: Jul. 23, 2021)

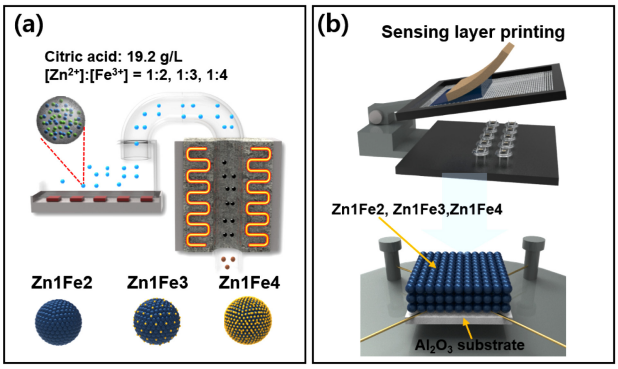

Fig. 1. Schematic of (a) material synthesis by ultrasonic spray pyrolysis and (b) fabrication of Zn1Fe2, Zn1Fe3, and Zn1Fe4 sensors.

[Zn]:[Fe] = 1:3, and 1:4 were prepared using the same method. However, different amounts of iron nitrate hexahydrate were used. For simplicity, the powders prepared from the solutions with [Zn]:[Fe] = 1:2, 1:3, and 1:4 will be referred to as Zn1Fe2, Zn1Fe3, and Zn1Fe4, respectively.

2.2 Sensor fabrication

The sensors were fabricated by screen printing of the slurries on alumina substrates (size: 1.5 × 1.5 mm^2) with two Au electrodes on the top surface and a micro-heater on the bottom surface (Fig. 1(b)). The slurries were prepared by dispersing the oxide powders in a terpineol-based ink vehicle (FCM, U.S.A). After screen printing, the sensors were annealed at 500 °C for 2 h to remove organic contents and to stabilize the sensors. For the measurement, the sensor was located into a small quartz tube (volume: 1.5 cm^3), and the atmosphere was controlled using a four-way valve to ensure a constant flow rate of 200 cm^3/min. The two-probe direct-current resistance of the sensors was measured using an electrometer (6487 Picoammeter, Keithley, USA) with a computer interface.

2.3 Characterization of sensing materials

The phase and crystallinity of the materials were analyzed using X-ray diffraction (XRD, D/MAX-2500 V/PC, Rigaku, Japan) with a Cu Ka radiation source (λ = 1.5418 Å). The micro/nanostructures and morphology of the materials and sensing films were observed using field-emission scanning electron microscopy (FE-SEM, S-4700, Hitachi Co. Ltd., Japan).

3. RESULTS AND DISCUSSIONS

The SEM images of Zn1Fe2, Zn1Fe3, and Zn1Fe4 powders are shown in Fig. 2. The powders exhibited spherical morphology and porous hollow structures. The mean diameters of Zn1Fe2, ZnFe3, and ZnFe4 spheres were 0.65 ± 0.20, 0.77 ± 0.23, and 0.85 ± 0.23 mm, respectively.

The phases of the samples were analyzed using X-ray diffraction (Fig. 3). Zn1Fe2 sample was identified as pure $ZnFe_2O_4$ spinel phase (ICDD# 89-1010) (Fig. 3(a)). The Zn1Fe3 and Zn1Fe4 samples were mixtures between a-Fe_2O_3 (ICDD # 84-0311) and $ZnFe_2O_4$ (Fig. 3(b,c)). From Scherrer's equation, the crystallite sizes of $ZnFe_2O_4$ in Zn1Fe2, Zn1Fe3, and Zn1Fe4 samples were calculated to be 21.1 ± 1.3, 20.2 3.2, and 19.8 ± 1.0 nm, respectively. Additionally, the crystallite sizes of a-Fe_2O_3 of Zn1Fe3, and Zn1Fe4 samples were 32.9 ± 4.6, and 34.4 ± 4.1 nm.

The gas sensing characteristics of Zn1Fe2, Zn1Fe3, and Zn1Fe4 sensors in the presence of 5 ppm ethanol, benzene, *p*-xylene, toluene, and CO within the temperature range of 275-350 °C were measured. All the sensors exhibited n-type gas sensing characteristics: the decrease in sensor resistance upon exposure to reducing gases and return of sensor resistance in air

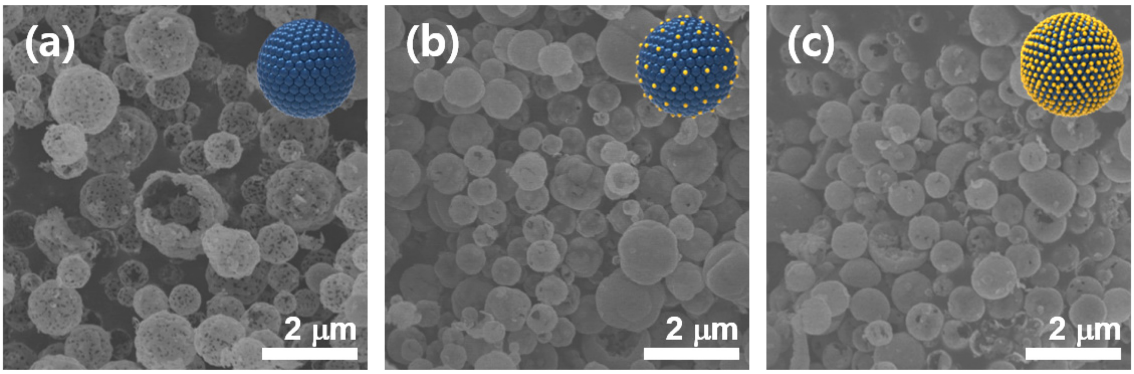

Fig. 2. SEM images of (a) Zn1Fe2 sensor, (b) Zn1Fe3 sensor, and (c) Zn1Fe4 sensor.

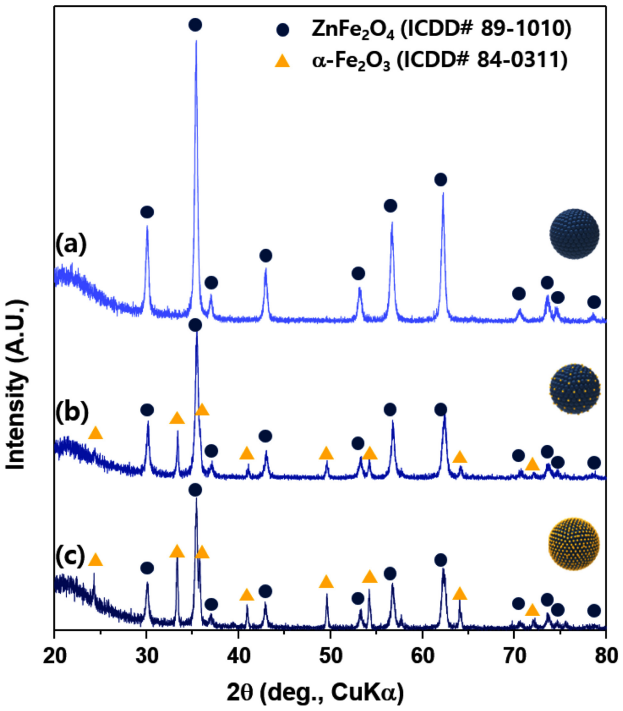

Fig. 3. X-ray diffraction patterns of (a) Zn1Fe2, (b) Zn1Fe3, and (c) Zn1Fe4 samples.

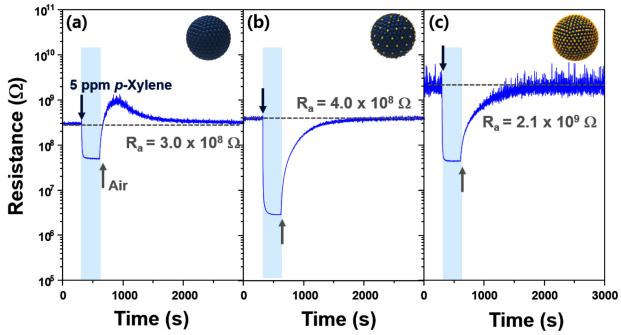

Fig. 4. Dynamic sensing transients of (a) Zn1Fe2, (b) Zn1Fe3, and (c) Zn1Fe4 sensors to 5 ppm p-xylene at 300 °C.

(Fig. 4). This is feasible considering the reports that $ZnFe_2O_4$ and Fe_2O_3 show n-type gas sensing characteristics [13,14]. Therefore, the gas response (S) was defined as R_a/R_g (R_a and R_g: resistance in air and gas).

The Zn1Fe2 sensor with pure $ZnFe_2O_4$ phase exhibited relatively low gas responses at 275 °C (Fig. 5(a)). Although the response to ethanol was the highest, the ethanol selectivity over other gases was insubstantial. In contrast, the Zn1Fe3 sensor composed of Fe_2O_3 and $ZnFe_2O_4$ showed significantly different gas sensing characteristics (Fig. 5(b)). The gas responses significantly increased and the gas selectivity was changed. For instance, the response to *p*-xylene at 275 °C (S = 220.6) is higher than that of ethanol (S = 152.1). The ethanol response decreased rapidly with an increase in sensing temperature to 300 °C, whereas the response to *p*-xylene gradually decreased, leading to the selective and sensitive detection of *p*-xylene at 300 °C. The higher responses to *p*-xylene over ethanol response were maintained at 325 °C. This suggests that the Zn1Fe3 sensor in the present study can be used to monitor ppm- and sub-ppm-level *p*-xylene, which is the most representative indoor/outdoor air pollutant emitted from varnishes, paint, rubber, ink, adhesives, and cleaning agents. The gas sensing characteristics of Zn1Fe4 sensor were measured at 300-350 °C since the sensor resistance at 275 °C was significantly high to measure (Fig. 5(c)). The sensor showed the highest

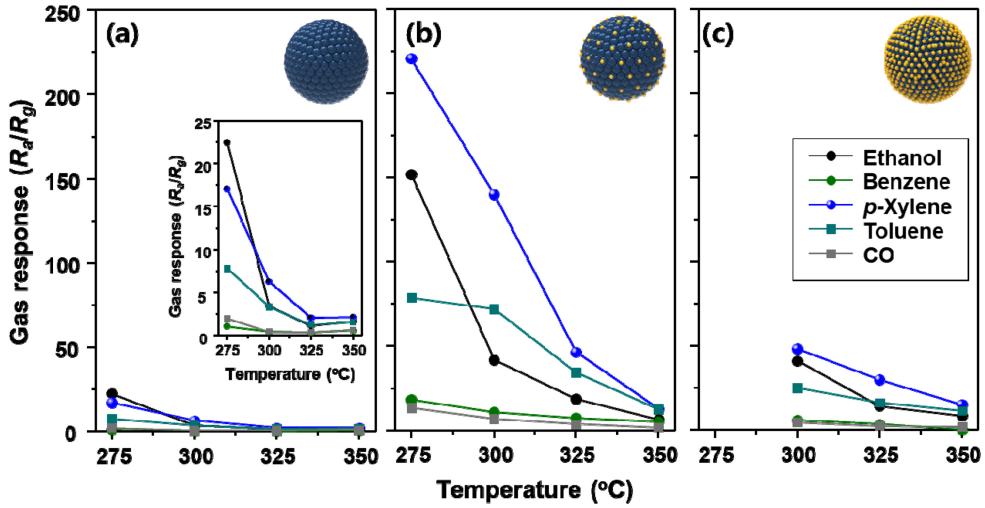

Fig. 5. Gas sensing characteristics of (a) Zn1Fe2 sensor, (b) Zn1Fe3 sensor, and (c) Zn1Fe4 sensor in the presence of 5 ppm of various gases (ethanol, benzene, p-xylene, toluene, and CO).

response to *p*-xylene.

In all the sensing materials, the diameters of spheres and crystallite sizes of $ZnFe_2O_4$ are similar. Therefore, the increase in gas response and the variation of selectivity should be discussed in association with the formation of α-Fe_2O_3 second phase. The high gas responses of Zn1Fe3 sensor can be explained partially by electronic sensitization. The work function of Fe_2O_3 is 5.88 eV [15], which is higher than that of $ZnFe_2O_4$ (4.56 eV) [16]. At the interface between $ZnFe_2O_4$ and α-Fe_2O_3, the electrons flow from $ZnFe_2O_4$ to Fe_2O_3, resulting in a lower charge carrier concentration in $ZnFe_2O_4$. This is supported by the higher R_a value in Zn1Fe3 than that in Zn1Fe2 (Fig. 4(a,b)). The sensor with lower background charge concentration exhibits a higher gas response when the same number of charges is provided from the sensing reaction. Considering the phase composition in Zn1Fe3 sensor, conduction is likely to occur along the larger amount of $ZnFe_2O_4$ phase. In this perspective, electronic sensitization, the decrease in charge carrier concentration in $ZnFe_2O_4$ due to the adjacent Fe_2O_3, can be a reason for the increase in gas response of Zn1Fe3 sensor. In the literature, the gas responses of $ZnFe_2O_4$-Fe_2O_3 heterostructures were higher than those of pure Fe_2O_3 [17,18]. Therefore, the decrease in gas response at 300 °C in Zn1Fe4 sensor might be explained by the formation of α-Fe_2O_3 phase.

The variation of gas selectivity is also associated with the formation of α-Fe_2O_3. α-Fe_2O_3 is known as a good catalyst to oxidize toluene and methylbenzene [19,20]. Furthermore, there have been reports on the enhancement of toluene selectivity either by doping Fe into NiO [21] or by decorating Fe_2O_3 nanorods on NiO nanotubes [22]. Accordingly, the different gas selectivity between Zn1Fe2 and Zn1Fe3 sensors can be attributed to the catalytic role of Fe_2O_3.

In ultrasonic spray pyrolysis, the droplets play the role of reaction containers. Therefore, well-defined hetero-composites with spherical morphology can be prepared, which provides a promising method to design high-performance gas sensors.

4. CONCLUSIONS

Highly sensitive and selective *p*-xylene sensors were fabricated using Fe_2O_3-$ZnFe_2O_4$ hetero-composite spheres prepared by ultrasonic spray pyrolysis. The pure $ZnFe_2O_4$ sensor exhibited neither high gas response nor selectivity towards a specific gas. In contrast, the Fe_2O_3-$ZnFe_2O_4$ hetero-composite sensor showed high gas response and selectivity to ppm-level *p*-xylene. The enhanced gas response was explained by the electronic sensitization of Fe_2O_3-$ZnFe_2O_4$ hetero-composite sensor due to the charge transfer from $ZnFe_2O_4$ to Fe_2O_3. The catalytic promotion of sensing reaction by Fe_2O_3 was suggested as the reason for the selectivity toward *p*-xylene.

ACKNOWLEDGMENTS

This work was supported by the National Research Foundation of Korea grants funded by the Korea government (2020R1A2 C3008933).

REFERENCES

[1] N. Yamazoe, “Toward innovations of gas sensor technology”, *Sens. Actuator B-Chem.*, Vol. 108, No. 1-2, pp. 2-14, 2005.

[2] H. J. Kim and J. H. Lee, “Highly sensitive and selective gas sensors using p-type oxide semiconductors: Overview”, *Sens. Actuator B-Chem.*, Vol. 192, pp. 607-627, 2014.

[3] B. Y. Kim, C. S. Lee, J. S. Park, and J.-H. Lee, “Preparation of Pt-, Ni- and Cr- Decorated SnO_2 Tubular Nanofibers and Their Gas Sensing Properties”, *J. Sens. Sci. Technol*, Vol. 23, No. 3, pp. 211-215, 2014.

[4] S. Y. Jeong, Y. M. Jo, Y. C. Kang, and J. H. Lee, “Xylene Sensor Using Cr-doped Co_3O_4 Nanoparticles Prepared by Flame Spray Pyrolysis”, *J. Sens. Sci. Technol.*, Vol. 29, No. 2, pp. 112-117, 2020.

[5] D. H. Kim, Y. S. Shim, and H. W. Jang, “Synthesis of Au-Decorated TiO_2 Nanotubes on Patterned Substrates for Selective Gas Sensor”, *J. Sens. Sci. Technol*, Vol. 23, No. 5, pp. 305-309, 2014.

[6] J. H. Lee, “Gas sensors using hierarchical and hollow oxide nanostructures: Overview”, *Sens. Actuator B-Chem.*, Vol. 140, No. 1, pp. 319-336, 2009.

[7] Y. M. Jo, T. H. Kim, C. S. Lee, K. R. Lim, C. W. N, F Abdel-Hady, A. A. Wazzan, and J. H. Lee, “Metal-organic framework-derived hollow hierarchical Co_3O_4 nanocages with tunable size and morphology: ultrasensitive and highly selective detection of methylbenzenes”, *ACS Appl. Mater. Interfaces*, Vol. 10, No. 10, pp. 8860-8868, 2018.

[8] H. J. Choi, J. H. Chung, J. W. Yoon, and J. H. Lee, “Highly selective, sensitive, and rapidly responding acetone sensor using ferroelectric ε-WO_3 spheres doped with Nb for monitoring ketogenic diet efficiency”, *Sens. Actuator B-Chem.*, Vol. 338, p. 129823, 2021.

[9] S. Y. Jeong, J. S. Kim, and J. H. Lee, “Rational Design of Semiconductor-Based Chemiresistors and their Libraries for Next-Generation Artificial Olfaction”, *Adv. Mater.*, Vol. 32, No. 51, p. 2002075, 2020.

[10] X. Chu., D. Jiang, G. Yu, and C. Zheng, “Ethanol gas sensor based on $CoFe_2O_4$ nano-crystallines prepared by hydrothermal method”, *Sens. Actuator B-Chem.*, Vol. 120, No. 1, pp. 177-181, 2006.

[11] B. Y. Kim, J. W. Yoon, K. Lim, S. H. Park, J. W. Yoon, and J. H. Lee, "Hollow spheres of $CoCr_2O_4$-Cr_2O_3 mixed oxides with nanoscale heterojunctions for exclusive detection of indoor xylene", *J. Mater. Chem. C*, Vol. 6, No. 40, pp. 10767-10774, 2018.

[12] D. S. Jung, S. B. Park, and Y. C. Kang, "Design of particles by spray pyrolysis and recent progress in its application", *Korean J. Chem. Eng.*, Vol. 27, No. 6, pp.1621-1645, 2010.

[13] X. Zhou, J. Liu, C. Wang, P. Sun, X. Hu, X. Li, K. Shimanoe, N. Yamazoe, and G. Lu, "Highly sensitive acetone gas sensor based on porous $ZnFe_2O_4$ nanospheres", *Sens. Actuator B-Chem.*, Vol. 206, pp. 577-583, 2015.

[14] H. J. Kim, K. I. Choi, A. Pan, I. D. Kim, H. R. Kim, K. M. Kim, C. W. Na, G. Cao, and J. H. Lee, "Template-free solvothermal synthesis of hollow hematite spheres and their applications in gas sensors and Li-ion Batteries", *J. Mater. Chem.*, Vol. 21, No. 18, pp.6549-6555, 2011.

[15] J. Liu, S. Yang, W. Wu, Q. Y. Tian, S. Cui, Z. Dai, and F. Ren, "3D Flowerlike α-Fe_2O_3@TiO_2 Core-Shell Nanostructures: General Synthesis and Enhanced Photocatalytic Performance", *ACS Sustain. Chem. Eng.*, Vol. 3, No. 11, pp. 2975-2984, 2015.

[16] X. Y. Liu, H. W. Zheng, Y. Li, and W. F. Zhang, "Factors on the Separation of Photogenerated Charges and the Charge Dynamics in Oxide/$ZnFe_2O_4$ Composites", *J. Mater. Chem. C*, Vol. 1, pp.329-337, 2013.

[17] Q. Ma, H. Li, Y. Liu, M. Liu, X. Fu, S. Chu, H. Li, and J. Guo, "Facile synthesis of flower-like α-Fe_2O_3/$ZnFe_2O_4$ architectures with self-assembled core-shell nanorods for superior TEA detection", *Curr. Appl. Phys.*, Vol. 21, pp.161-169, 2021.

[18] Q. Wei, J. Sun, P. Song, J. Li, Z. Yang, and Q. Wang, "Spindle-like Fe_2O_3/$ZnFe_2O_4$ porous nanocomposites derived from metal-organic frameworks with excellent sensing performance towards triethylamine", *Sens. Actuator B-Chem.*, Vol. 317, p. 128205, 2020.

[19] W. Han, J. Deng, S. Xie, H. Yang, H. Dai, and C.T. Au, "Gold supported on iron oxide nanodisk as efficient catalyst for the removal of toluene", *Ind. Eng. Chem. Res.*, Vol. 53, No. 9, pp. 3486-3494, 2014.

[20] J. Ouyang, J. Pei, Q. Kuang, Z. Xie, and L. Zheng, "Supersaturation-controlled shape evolution of a-Fe_2O_3 nanocrystals and their facet- dependent catalytic and sensing properties", *ACS Appl. Mater. Interfaces*, Vol. 6, No. 15, pp. 12505-12514, 2014.

[21] J. M. Suh, Y. S. Shim, D. H. Kim, W. Sohn, Y. Jung, S. Y. Lee, S. Choi, Y. H. Kim, J. M. Jeon, K. Hong, K. C. Kwon, S. Y. Park, C. Kim, J. H. Lee, C. Y. Kang, H. W. Jang, "Synergetically Selective Toluene Sensing in Hematite-Decorated Nickel Oxide Nanocorals", *Adv. Mater. Technol.*, Vol. 2, No. 3, p. 1600259, 2017.

[22] C. Wang, T. Wang, B. Wang, X. Zhou, X. Cheng, P. Sun, J. Zheng, and G. Lu, "Design of a-Fe_2O_3 nanorods functionalized tubular NiO nanostructure for discriminating toluene molecule", *Sci. Rep.*, Vol. 6, p. 26432, 2016.